Computers and Geotechnics 135 (2021) 104168

Contents lists available at ScienceDirect

Computers and Geotechnics

journal homepage: www.elsevier.com/locate/compgeo

Research Paper

A half-space based contact detection algorithm for complex blocks

Xinquan Wang [a,b], Chun Feng [a,b,*], Xinguang Zhu [a,b], Li Zhang [a], Shihai Li [a,b]

[a] Institute of Mechanics, Chinese Academy of Sciences, Beijing 100190, China
[b] School of Engineering Science, University of Chinese Academy of Sciences, Beijing 100049, China

ARTICLE INFO

Keywords:
Contact detection
Potential contact pair
Half-space inclusion relation
Convex polygonal block
Convex polyhedral block

ABSTRACT

Contact detection algorithm is a critical constituent of discontinuous calculation method, the accuracy of contact detection directly affects the simulation results. Algorithms for contact detection between irregular blocks are difficult to achieve because of the complexity of geometry and the diversity of contact types. A half-space based contact detection algorithm is proposed, it can accurately identify the contact relationship between convex polygonal and polyhedral blocks. The proposed contact detection approach is implemented into continuum-discontinuum element method. This contact detection algorithm consists of two stages: first to identify potential contact pairs and then to judge the contact status by half-space. Half-space is defined by the boundary of the block, by judging the half-space inclusion relation between potential contact pairs, the contact status between two blocks can be detected, there is no need to calculate the distance between blocks in the process of contact state detection. This algorithm is realized through programming, several examples validated the accuracy of this algorithm.

1. Introduction

Contact detection plays an important role in virtual reality (Bovet et al., 2018; Garbaya and Zaldivar-Colado, 2007; Zhang et al., 2007), robot motion planning (Barraquand and Latombe, 1991; Aceituno et al., 2018), engineering analysis (Redon et al., 2010; Marques et al., 2020), numerical simulation (Park and Song, 2009; Tan et al., 2016; Mai et al., 2017) and other fields (Yang et al., 2020; Khishvand et al., 2017). Contact detection algorithm is important to numerical simulation of geological hazards, for landslides (Davies and McSaveney, 2009) and debris flows (Coussot and Meunier, 1996), a large number of irregular rock mass contact during their movement, blocks contact with neighbor blocks thus changing the motion patterns. The contact state is changed and needs to be updated for numerical simulations consider the interaction of different blocks.

Contact detection are widely used in discontinue calculation, such as discrete element method (DEM) (Cundall, 1971), continuum discontinuum element method (CDEM) (Li et al., 2015; Zhang et al., 2020) and discontinuous deformation analysis (DDA) (Hatzor et al., 2017; Shi, 1992). In recent years, continuous-discontinuous coupling numerical simulation methods have been widely used in solid collisional crushing field (Lin et al., 2021). The accurate description of the fracture cracking process (Zhang et al., 2020; Zhang and Zhuang, 2018; Mu and Zhang, 2020; Zhang and Zhuang, 2019; Zhang and Mang, 2020) and high-precision contact detection methods between complex blocks are the challenges of continuous-discontinuous coupling methods. Rigorous contact detection algorithm is necessary for numerical methods considering the discrete characteristics of blocks. The accuracy of contact detection directly affects the reliability of the numerical simulation results.

DEM using spheres to simulate the movement of objects in the early stage (Cundall and Strack, 1979), the contact relationship between spheres can be directly judged by the distance between centers, and the contact detection algorithm is simple. Since it is difficult for spherical particles to express the true shape of irregular objects, the interactions of objects during the movement process are hard to simulate. With the development of discrete elements, irregular elements such as ellipsoid (Zhou et al., 2018; Peng and Hanley, 2019; Römer et al., 2018), polygonal and polyhedral blocks (Boon et al., 2012; Boon et al., 2013; Stühler et al., 2016; Wu, 2008) have been developed. Irregular elements are more suitable to simulate objects in the real world. However, due to the complexity of geometry and the diversity of contact types, algorithms for complete contact identification and efficient contact retrieval between irregular blocks are difficult to achieve.

The contact algorithm is the most time-consuming part of the discrete element calculation (Shire et al., 2020; Lubbe et al., 2020),

* Corresponding author at: Institute of Mechanics, Chinese Academy of Sciences, Beijing 100190, China.
E-mail address: fengchun@imech.ac.cn (C. Feng).

https://doi.org/10.1016/j.compgeo.2021.104168
Received 26 November 2020; Received in revised form 17 March 2021; Accepted 11 April 2021
Available online 5 May 2021

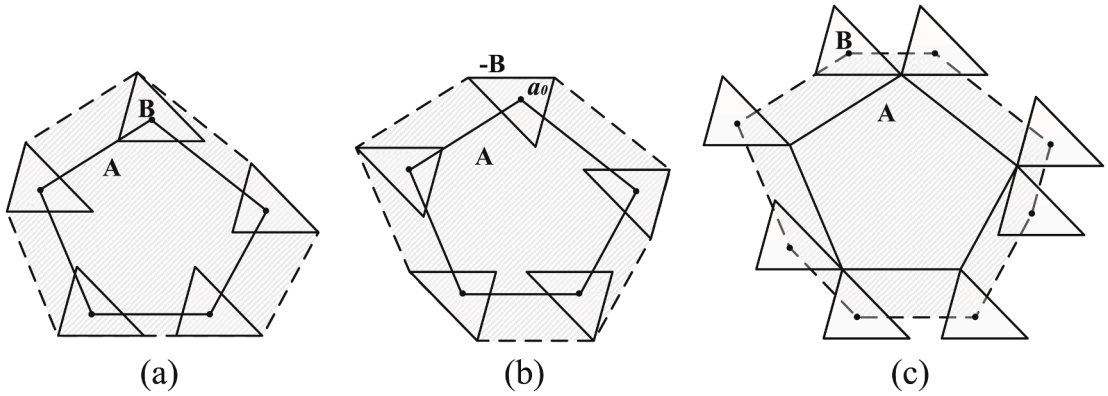

Fig. 1. The Minkowski sum of A and B.

contact relationship between blocks needs to be identified and updated constantly during the calculation process. Neighbor search is a rough contact search (Liu and Lemos, 2001; Zhong and Nilsson, 1989) aim to find blocks in close proximity to each other that have possible to contact, it can greatly reduce the number of blocks that need to be detected (Wang et al., 2020; Wang et al., 2019). Then use delicate search to determine whether those blocks screened out by the neighbor search are contact or not. Delicate search is aim to determine the specific contact status and contact relationship between two blocks, the accuracy of this method is highly requirement.

There are numerous methods for delicate contact detection. The common plane (CP) method (Cundall, 1988) detect two blocks contact status by judging whether there is a common plane between them. The efficiency of CP is highly dependent on the initially common plane normal. The fast common plane (FCP) (Nezami et al., 2004) algorithm and the shortest link method (SLM) (Nezami et al., 2006) can improve CP efficiency by reduce the search space for the common plane. The semi-spring and semi-edge contact model (Feng et al., 2014) and the shrunken edge algorithm (Wang et al., 2015) are useful to detect relationship between neatly stacked blocks. However, the contact status is usually judged by the distance between blocks, when the distance between blocks is less than the tolerance value, the two blocks are recognized as contact. The calculation of the nearest distance between blocks is complicated, and the contact status between blocks is influenced by the tolerance value, which may lead to misjudgment. Recently, a rigid contact theory named the entrance block theory (Shi, 2015) transforms the contact relationship between two blocks into the contact relationship between a point and a block, it provides an efficient contact detection method. Contact detection algorithms based on this theory (Zhuang et al., 2020; Zheng et al., 2019; Zheng et al., 2018a; Zheng et al., 2017a; Wang et al., 2020; Jafari and Keneti, 2013; Zhang et al., 2016; Fan et al., 2018; Zheng et al., 2017b; Zheng et al., 2018b) are widely used in DDA. For irregular blocks (e.g., blocks with small angles or edges), the contact force are obtained by the potential-based penalty function approach (Zheng et al., 2020a; Zheng et al., 2020b) show good robustness and efficiency.

A half-space based contact detection algorithm is proposed in this paper, this algorithm is based on the entrance block theory. Two basic conception are defined for the contact detection: potential contact pair and half-space inclusion relation. This paper uses explicit solution approach to solve the block movement, two blocks are considered as contact when they have an overlapping area. The contact status between two blocks is judged by the half-space inclusion relation of potential contact pair. Potential contact pairs are identified through the relationship between the surface normal vector and the common vertex vectors. Half-space inclusion relation is determined by judging whether one block is located in the half-space divided by the outer boundary of the other block. The contact relationship between convex blocks can be identified thought this algorithm.

This paper is organized as follow. Section 2 provides the theoretical basis of contact detection, and introduces the contact detection algorithm for two-dimensional (2D) and three-dimensional (3D) blocks. Section 3 introduces the contact force calculation method. Section 4 verifies the robustness and accuracy of the algorithm through several examples. The main conclusions are drawn in Section 5.

2. Contact detection algorithm

In Section 2.1, the basic theory for contact detection is introduced. The newly developed algorithm for contact detection is then described in Section 2.2 based on this prior knowledge. The contact detection algorithm for convex polygonal and polyhedral blocks are proposed in Section 2.3 and Section 2.4 respectively. Section 2.5 introduces the recognition of contact type.

2.1. Basic theory

2.1.1. Minkowski sum

Given two blocks A and B, the Minkowski sum (Varadhan and Manocha, 2006; Bekker and Roerdink, 2001; Barki et al., 2009) of A and B is defined as a set with the sum of all pairs of points in A and B:

$$A + B = \{a + b | a \in A, b \in B\}, \tag{1}$$

where a is the point from A, and b is the point from B.

The Minkowski sum of A and B is the sum of A and B, it can be obtained by sweeping one block B (with a fixed orientation) along the other block A (see Fig. 1(a)). Minkowski Sum of convex blocks is still a convex block.

Denoted -B as the symmetric block of B with respect to the origin, the Minkowski sum of A and -B is:

$$A + (-B) = \{a + (-b) | a \in A, b \in B\}. \tag{2}$$

From the above statement, the Minkowski sum of A and -B can be obtained by sweeping -B along A (see Fig. 1(b)). If the region contains the origin, it means A and B have points with same coordinates, and there is contact between A and B (Gilbert et al., 1987). Through Minkowski sum, the contact problem between A and B is transformed into the problem of whether the Minkowski sum of A and -B contains the origin.

The Minkowski sum of A and -B can also be obtained by moving B around the outer boundary of A, and tracking the movement path of a fixed point in B (see Fig. 1(c)). The tracking point is defined as the reference point. If the reference point is located in the Minkowski sum region of A and -B, the two blocks have points with the same coordinates and there is contact between A and B. The contact relationship between A and B is transformed into the relationship between the reference point and the Minkowski sum of A and -B.

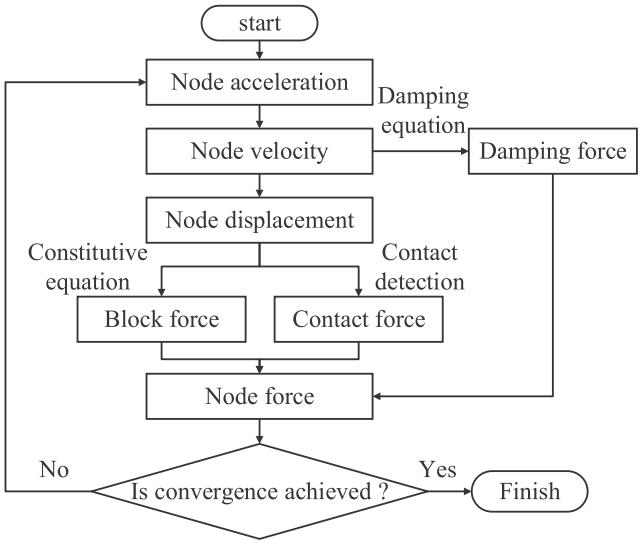

Fig. 2. Calculation flowchart of CDEM.

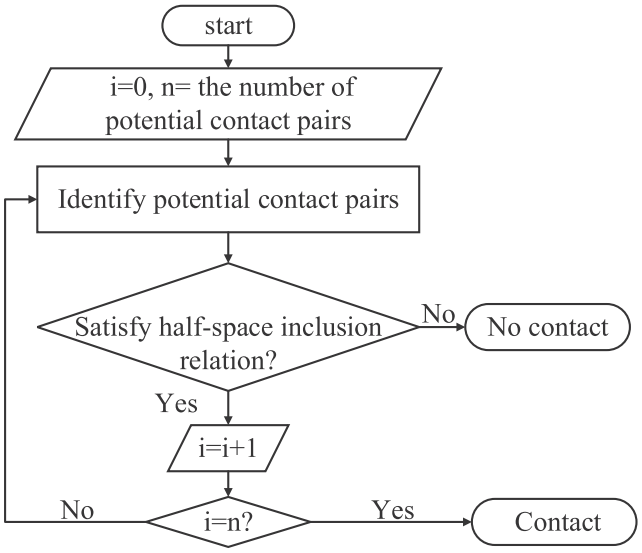

Fig. 3. Flowchart of contact detection.

2.1.2. Entrance block theory

The entrance block theory use Minkowski Sum for algebraic operations of blocks (Shi, 2015). For block A and block B, given a reference point a_0 on block A. The relationship between A and B transfer to the relationship between a_0 and entrance block $E(A,B)$. Entrance block $E(A,B)$ is defined as:

$$E\left(A,B\right)=\bigcup_{a\in A,b\in B}\left(b-a+a_0\right)=B-A+a_0. \tag{3}$$

If A and B are 2D convex polygons, the boundary of $E(A,B)$ is $\partial E(A,B)$, which is defined as:

$$\partial E(A,B)=C(0,1)\cup C(1,0), \tag{4}$$

where $C(0,1)$ is the set of contact edges formed by the points of block $A$and the edges of block B, $C(1,0)$ is the set of contact edges formed by the edges of block $A$and the points of block B.

If $A$and $B$are 3D convex polyhedrons, the boundary of $E(A,B)$ is $\partial E(A,B)$, which is defined as:

$$\partial E(A,B)=C(0,2)\cup C(2,0)\cup C(1,1), \tag{5}$$

where $C(0,2)$ is the set of contact polygons formed by the points of block $A$and the surface of block B, $C(2,0)$ is the set of contact polygons formed by the faces of block $A$and the points of block B, $C(1,1)$ is the collection of the contact polygons formed by the edge of block $A$and the edge of block B.

2.1.3. Continuum-discontinuum element method

In this paper, the movement of blocks are calculated using continuum-discontinuum element method (CDEM). CDEM is an explicit solution approach based on finite difference principles, FEM and DEM are combined in this method, and forward-difference approximation is adopted to calculate the progressive process (Feng et al., 2014). Convergence is achieved in a reasonable time with small time steps using the dynamic relaxation method.

The calculation flowchart of the CDEM is shown in Fig. 2. Contact forces are calculated by using the contact algorithm in this paper. By using small time steps, the maximum displacement in one step is limited to be smaller than the smallest edge in the block system. The influence of blocks with small edges or small angles on contact detection can be eliminated.

2.2. Contact detection based on the half-space

When the outer boundaries of two blocks are in touch or when there is an overlap of two blocks, the two blocks are considered to be in contact. Two blocks are considered to be in initial contact relationship when their outer boundaries are in contact, the contact geometry elements in initial contact blocks are contact pairs. Identifying potential contact pairs and detecting the relationship of potential contact pairs can simplify the detection progress. Considering the process of constructing the Minkowski sums of two blocks, one block is moving around the boundary of the other. Position relationships between two blocks when they constructing a Minkowski sum can be considered as the set of their initial contact position, the contact geometry elements when one block is moving around the other block are contact pairs. There are certain conditions between contact pairs, taking polygons for example, the Minkowski sum of two polygons is constructed by moving vertices along edges. When the direction vectors of the vertex point outside from edge, the vertex can move along the edge, then the vertex and the edge can be considered as contact pairs.

Two basic conceptions are proposed in this algorithm for the contact detection between two blocks: potential contact pairs and half-space inclusion relation. Geometry elements from different blocks have the possibility to contact first are defined as potential contact pairs. The relative relation between the two geometry elements in potential contact pair is half-space inclusion relation. This contact detection algorithm determines contact status between two blocks by detecting the half-space inclusion relation of potential contact pairs, Fig. 3 presents the procedure of contact detection.

For polygons, the contact type can be divided into vertex-vertex contact, vertex-edge contact and edge-edge contact. There must be vertex-edge contact when two blocks have vertex-vertex contact or edge-edge contact. Therefore, all three types of contact can be attributed to vertex-edge contact (see Fig. 4(a)). The contact detection of polygons requires the identification of vertex-edge potential contact pairs. The half-space inclusion relation of vertex and edge is the relative relation of vertex and edge in potential contact pair. It is determined by judging whether the vertex is located in the half-space defined by the edge.

For polyhedrons, the contact type can be divided into vertex-vertex contact, vertex-edge contact, vertex -face contact, edge-edge contact, edge-face contact and face-face contact. In the process of contact detection, the above six contact types can be summarized into two basic contact types: vertex-face contact and edge-edge contact (see Fig. 4(b), Fig. 4(c)). Therefore, there are vertex-face potential contact pairs and

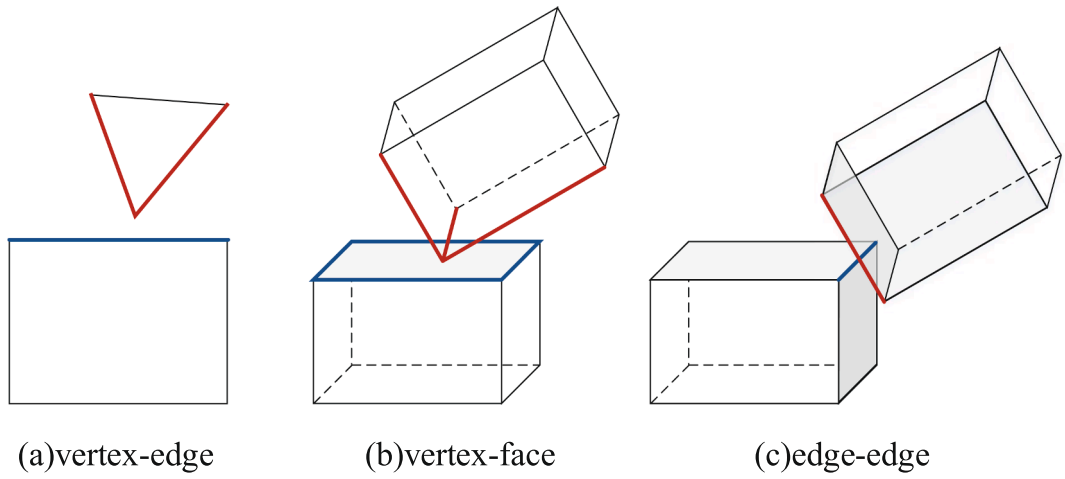

Fig. 4. Basic contact types.

edge-edge potential contact pairs in polyhedrons contact detection. The half-space inclusion relation of vertex and face is the relative relation of vertex and face in vertex-face potential contact pair. It is determined by judging whether the vertex is located in the half-space defined by the face. The half-space inclusion relation of edge and edge is the relative relation of two edges in edge-edge potential contact pair. It is determined by judging whether the edge is located in the half-space defined by those two edges.

The identification of potential contact pairs and their relative position relationships can be achieved through vector calculations. It does not require the calculation of the distance between blocks in the process of contact status determination. The specific contact algorithm is discussed in detail in Section 2.3.

2.3. Contact detection algorithm for convex polygonal blocks

2.3.1. Geometrical description of convex polygon

A convex polygon is defined as a simple polygon (not self-intersecting) with all interior angles less than 180°. A convex polygon can be defined by the set of its vertices. A convex n-polygon Acan be stated as:

$$A = e_i e_{i+1} \ldots e_n, \tag{6}$$

where $e_i (i = 1, \ldots, n)$ is the vertex of polygon A. There are two direction vectors for this vertex, respectively $\overrightarrow{e_i e_{i+1}}$ and $\overrightarrow{e_i e_{i-1}}$. The edge with vertices e_i and e_j is denoted as $e_i e_j$. Vertex is the intersection point of two edges, normal vector of edge $e_i e_j$ is represented as $\overrightarrow{n_{ij}}$.

Each edge of a convex polygon can define a half-space. For an edge with normal vector $\overrightarrow{n_1}$, given a point a_1 on the edge, the half-space defined by this edge can be represented as:

$$(p - a_1) \cdot \overrightarrow{n_1} \geqslant 0, \tag{7}$$

where $p$is a point in the half-space. The convex polygon is completely in a half-space defined by each of its edge.

The convex polygon is the intersection of all that half-spaces. A convex n-polygon can be defined as

$$(p - a_i) \cdot \overrightarrow{n_i} \geqslant 0 \quad (i = 1, \ldots, n), \tag{8}$$

where a_i is the point on the ith edge of polygon, and n_i is the normal vertex of the ith edge.

2.3.2. Vertex-edge potential contact pair

For polygon $A$and polygon B, denote e_i as a vertex of A, $\overrightarrow{e_i e_{i-1}}$ and $\overrightarrow{e_i e_{i+1}}$ are two direction vectors of this vertex respectively. Denote $e_j e_k$ as a edge of B, $\overrightarrow{n_{jk}}$ is the inner normal vector of this edge. If vertex e_i and edge $e_j e_k$ satisfy:

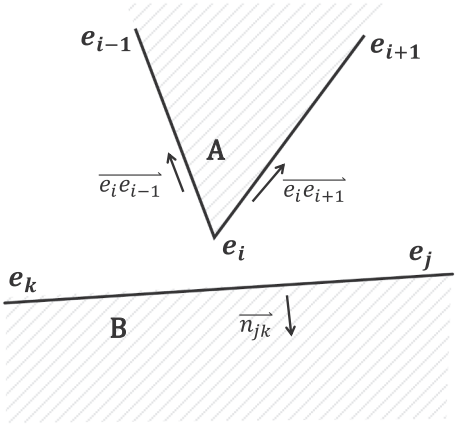

Fig. 5. Vertex-edge potential contact pair.

$$\overrightarrow{e_i e_{i-1}} \cdot \overrightarrow{n_{jk}} \leqslant 0, \overrightarrow{e_i e_{i+1}} \cdot \overrightarrow{n_{jk}} \leqslant 0, \tag{9}$$

then the vertex e_i and the edge $e_j e_k$ is defined as vertex-edge potential contact pair(see Fig. 5).

2.3.3. Half-space inclusion relation of vertex and edge

For a vertex-edge potential contact pair with vertex e_i form polygon A and edge $e_j e_k$ from polygon B, $\overrightarrow{n_{jk}}$ is the inner normal vector of this edge. If the relation between vertex e_i and edge $e_j e_k$ satisfy

$$\overrightarrow{e_i p_i} \cdot \overrightarrow{n_{jk}} \leqslant 0, \tag{10}$$

where $\overrightarrow{e_i p_i}$ is the direction vector of the line form e_i to a point p_i on the edge $e_j e_k$. Then the vertex e_i is locate inside the half-space defined by the edge $e_j e_k$. The vertex-edge potential contact pair satisfies the half-space inclusion relation.

For blocks that are initially stacked neatly, they are in contact with their neighbors blocks along their boundaries. All contact pairs satisfy the half-space inclusion relation at the first time step. In that case, initial contact pairs can not be recognized properly by conventional methods.

To deal with this problems, the tolerance to define half-space inclusion relation is altered in the first step, Eq. (10) is changed into

$$\overrightarrow{e_i p_i} \cdot \overrightarrow{n_{jk}} < 0. \tag{11}$$

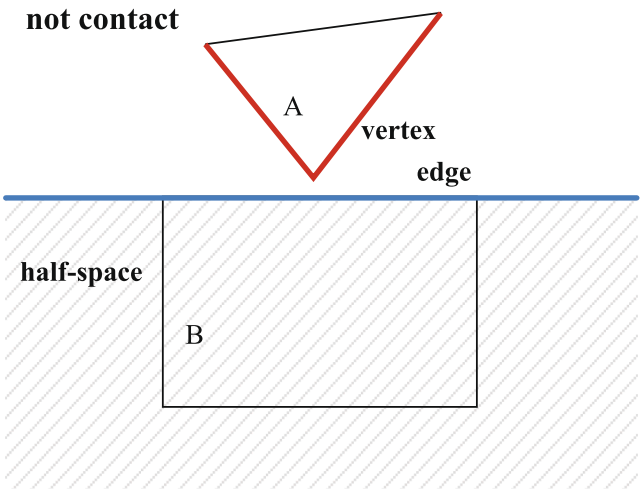

Fig. 6. Vertex located outside the edge.

In this way, adjacent blocks are not recognized as contact, thus forming initial contact pairs.

2.3.4. Contact detection

As shown in Fig. 6, for convex polygons, if the vertex is located outside the half-space defined by edge, there is no possibility of contact between *A*and *B*. If the vertex is located inside the half-space, there is a possibility of contact. That is

$$\neg(\exists \text{ Satisfy half} - \text{space inclusion relation}) \Rightarrow \neg \text{ Contact}. \tag{12}$$

Consider the relationship between original proposition and converse-negative proposition:

$$\text{Contact} \Rightarrow \forall \text{ Satisfy half} - \text{space inclusion relation}. \tag{13}$$

Form above discussion, for polygons, all the contact types can be attributed to vertex-edge contact, it means there are only vertex-edge potential contact pairs in polygons. When two blocks do not contact, there must be vertex-edge potential contact pairs do not satisfy the half-space inclusion, that is

$$\neg \text{ Contact} \Rightarrow \neg(\exists \text{Satisfy half} - \text{space inclusion relation}). \tag{14}$$

By the relation between original proposition and converse-negative proposition:

$$\forall \text{ Satisfy half} - \text{space inclusion relation} \Rightarrow \text{Contact}. \tag{15}$$

In conclusion

$$\forall \text{ Satisfy half} - \text{space inclusion relation} \Leftrightarrow \text{Contact}. \tag{16}$$

If all vertex-edge potential contact pairs between the two blocks satisfy the half-space inclusion, the two blocks are in contact. If there are vertex-edge potential contact pairs do not satisfy the half-space inclusion, the two blocks are not in contact. In contact status judgment, only when the previous vertex-edge potential contact pair satisfy the half-space inclusion relation, the next vertex-edge potential contact pair is judged, which saves the time of contact detection.

The contact status of two blocks is judged by the above method, and the contact relationship can be identified when the contact occurs. The vertex-vertex contact, vertex-edge contact and edge-edge contact are identified after two blocks are judged to be in contact, the contact type is judged according to the position of the contact, and the corresponding contact force is applied.

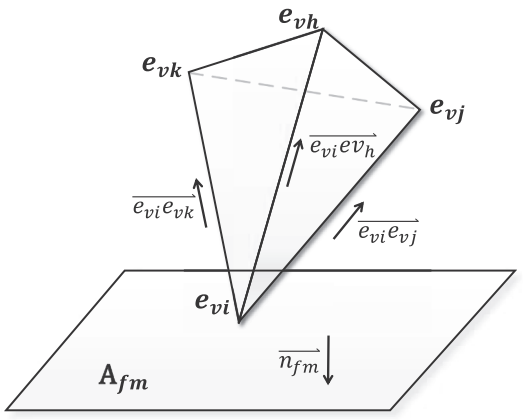

Fig. 7. Vertex-face potential contact pair.

2.4. Contact detection algorithm for convex polyhedral blocks

2.4.1. Geometrical description of convex polyhedron

A convex polyhedron is a 3D object with flat polygonal faces, straight edges and sharp corners or vertices. Faces of polyhedron are the polygons cover the polyhedron. The common edge of two faces is the edge of the polyhedron, and the common point of edges is the vertex of the polyhedron.

The face of the polyhedron is denoted as A_{fi}, the inner normal vector of face A_{fi} is denoted as $\overrightarrow{n_{fi}}$. Edge $e_{vi}e_{vj}$ is the intersection of face A_{fm} and A_{fn}, the direction vector of this edge is $\overrightarrow{e_{vi}e_{vj}}$, the vertices at the ends of the edge are e_{vi} and e_{vj} respectively. Vertex is the intersection point of different edges. Vertex e_{vi} is the intersection point of edge $e_{vi}e_{vj}$, …and edge $e_{vi}e_{vk}$, the direction vectors of this vertex are $\overrightarrow{e_{vi}e_{vj}}$, …and $\overrightarrow{e_{vi}e_{vk}}$.

Each face of a convex polyhedron can define a half-space. For an face with normal vector $\overrightarrow{n_1}$, given a point a_1 on the face, the half-space defined by this face can be represented as

$$(p - a_1)\cdot\overrightarrow{n_{f1}} \geqslant 0, \tag{17}$$

where *p*is point in the half-space. The convex polyhedron is completely in a half-space defined by each of its face.

The convex polyhedron is the intersection of all that half-spaces. A convex n-polyhedron can be defined as

$$(p - a_i)\cdot\overrightarrow{n_{fi}} \geqslant 0 \quad (fi = 1, \ldots, n), \tag{18}$$

where a_i is the point on the *i*th face of polyhedron, and n_i is the normal vertex of the *i*th face.

2.4.2. Vertex-face potential contact pair

For polyhedron Ω_1 and polyhedron Ω_2, e_{vi} is a vertex of Ω_1, direction vectors of this vertex are $\overrightarrow{e_{vi}e_{vj}}$, …, $\overrightarrow{e_{vi}e_{vk}}$ respectively. A_{fm} is a face of Ω_2, $\overrightarrow{n_{fm}}$ is the inner normal vector of this face. If vertex e_{vi} and face A_{fm} satisfy:

$$\overrightarrow{e_{vi}e_{vj}}\cdot\overrightarrow{n_{fm}} \leqslant 0, \ldots, \overrightarrow{e_{vi}e_{vk}}\cdot\overrightarrow{n_{fm}} \leqslant 0, \tag{19}$$

then the vertex e_{vi} and the face A_{fm} is defined as vertex-face potential contact pair(see Fig. 7).

2.4.3. Edge-edge potential contact pair

Given two polyhedrons Ω_1 and Ω_2, $e_{vi}e_{vj}$ is a edge of Ω_1 and $e_{vk}e_{vm}$ is a edge of Ω_2. $e_{vi}e_{vj}$ is the intersection of face A_{fi} and A_{fj}, the direction vector of edge $e_{vi}e_{vj}$ is $\overrightarrow{e_{vi}e_{vj}}$, the inner normal vector of face A_{fi} is $\overrightarrow{n_{fi}}$, the inner normal vector of face A_{fj} is $\overrightarrow{n_{fj}}$. $e_{vk}e_{vm}$ is the intersection of face A_{fk} and A_{fm}, the direction vector of edge $e_{vk}e_{vm}$ is $\overrightarrow{e_{vk}e_{vm}}$, the inner normal

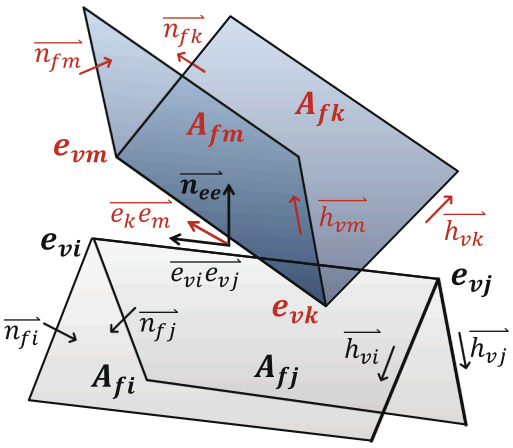

Fig. 8. Edge-edge potential contact pair.

vector of face A_{fk} is $\overrightarrow{n_{fk}}$, the inner normal vector of face A_{fm} is $\overrightarrow{n_{fm}}$.

Direction vectors normal to edge $e_{vi}e_{vj}$ in face A_{fi} and face A_{fj} are $\overrightarrow{h_{vi}}$ and $\overrightarrow{h_{vj}}$ respectively, which are computed as

$$\overrightarrow{h_{vi}} = \overrightarrow{e_{vi}e_{vj}} \times \overrightarrow{n_{fi}},\ \overrightarrow{h_{vj}} = \overrightarrow{n_{fj}} \times \overrightarrow{e_{vi}e_{vj}}. \tag{20}$$

Direction vectors normal to edge $e_{vk}e_{vm}$ in face A_{fk} and face A_{fm} are $\overrightarrow{h_{vk}}$ and $\overrightarrow{h_{vm}}$ respectively, which are computed as

$$\overrightarrow{h_{vk}} = \overrightarrow{e_{vk}e_{vm}} \times \overrightarrow{n_{fk}},\ \overrightarrow{h_{vm}} = \overrightarrow{n_{fm}} \times \overrightarrow{e_{vk}e_{vm}}. \tag{21}$$

When move edge $e_{vi}e_{vj}$ and edge $e_{vk}e_{vm}$ to the same plane, define $\overrightarrow{n_{ee}}$ as the normal vector of this plane:

$$\overrightarrow{n_{ee}} = \overrightarrow{e_{vk}e_{vm}} \times \overrightarrow{e_{vi}e_{vj}}. \tag{22}$$

If

$$\overrightarrow{n_{ee}} \times \overrightarrow{h_{vi}} \leqslant 0,\ \overrightarrow{n_{ee}} \times \overrightarrow{h_{vj}} \leqslant 0,\ \overrightarrow{n_{ee}} \times \overrightarrow{h_{vk}} \geqslant 0,\ \overrightarrow{n_{ee}} \times \overrightarrow{h_{vm}} \geqslant 0, \tag{23}$$

or

$$\overrightarrow{n_{ee}} \times \overrightarrow{h_{vi}} \geqslant 0,\ \overrightarrow{n_{ee}} \times \overrightarrow{h_{vj}} \geqslant 0,\ \overrightarrow{n_{ee}} \times \overrightarrow{h_{vk}} \leqslant 0,\ \overrightarrow{n_{ee}} \times \overrightarrow{h_{vm}} \leqslant 0, \tag{24}$$

then edge $e_{vi}e_{vj}$ and edge $e_{vk}e_{vm}$ is edge-edge potential contact pair (see Fig. 8).

2.4.4. Half-space inclusion relation of vertex and face

After identifying vertex-face potential contact pairs and edge-edge potential contact pairs, the half-space inclusion relation between vertex and face in vertex-face potential contact pairs and the half-space inclusion relation between edge and edge in edge-edge potential contact pairs are detected.

For a vertex-face potential contact pair with vertex e_{vi} form polyhedron Ω_1 and face A_{fk} from polyhedrons Ω_2, the inner normal vector of face A_{fk} is $\overrightarrow{n_{fk}}$. If the relation between vertex e_{vi} and face A_{fk} satisfy

$$\overrightarrow{e_{vi}p_i} \cdot \overrightarrow{n_{fk}} \leqslant 0, \tag{25}$$

where $\overrightarrow{e_{vi}p_i}$ is the direction vector of the line form e_{vi} to a point p_i on the face A_{fk}. Then the vertex e_{vi} is locate inside the half-space defined by the face A_{fk}. The vertex-edge potential contact pair satisfies the half-space inclusion relation.

For blocks that are initially stacked neatly, the tolerance to define half-space inclusion relation is altered in the first step, Eq. (25) is changed into

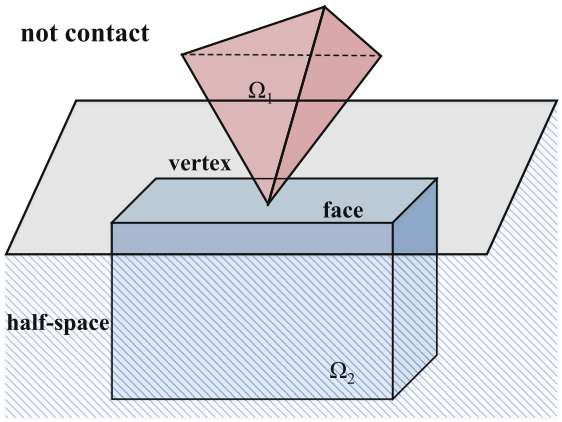

Fig. 9. Vertex located outside the face.

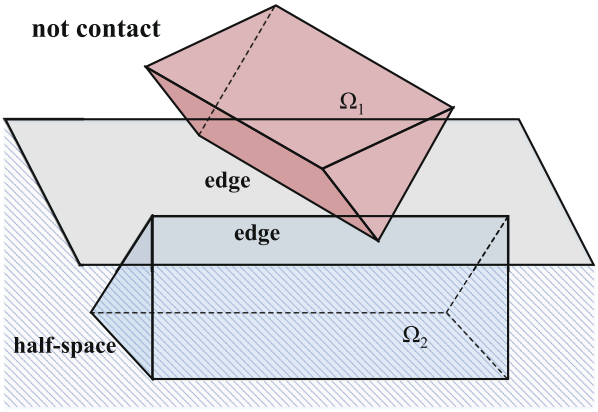

Fig. 10. Edge located outside the edge.

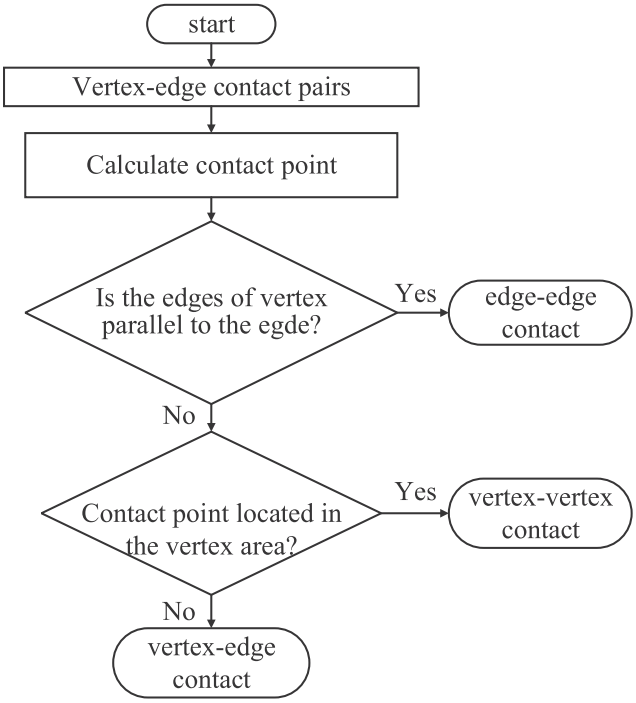

Fig. 11. Contact type recognition in 2D polygons.

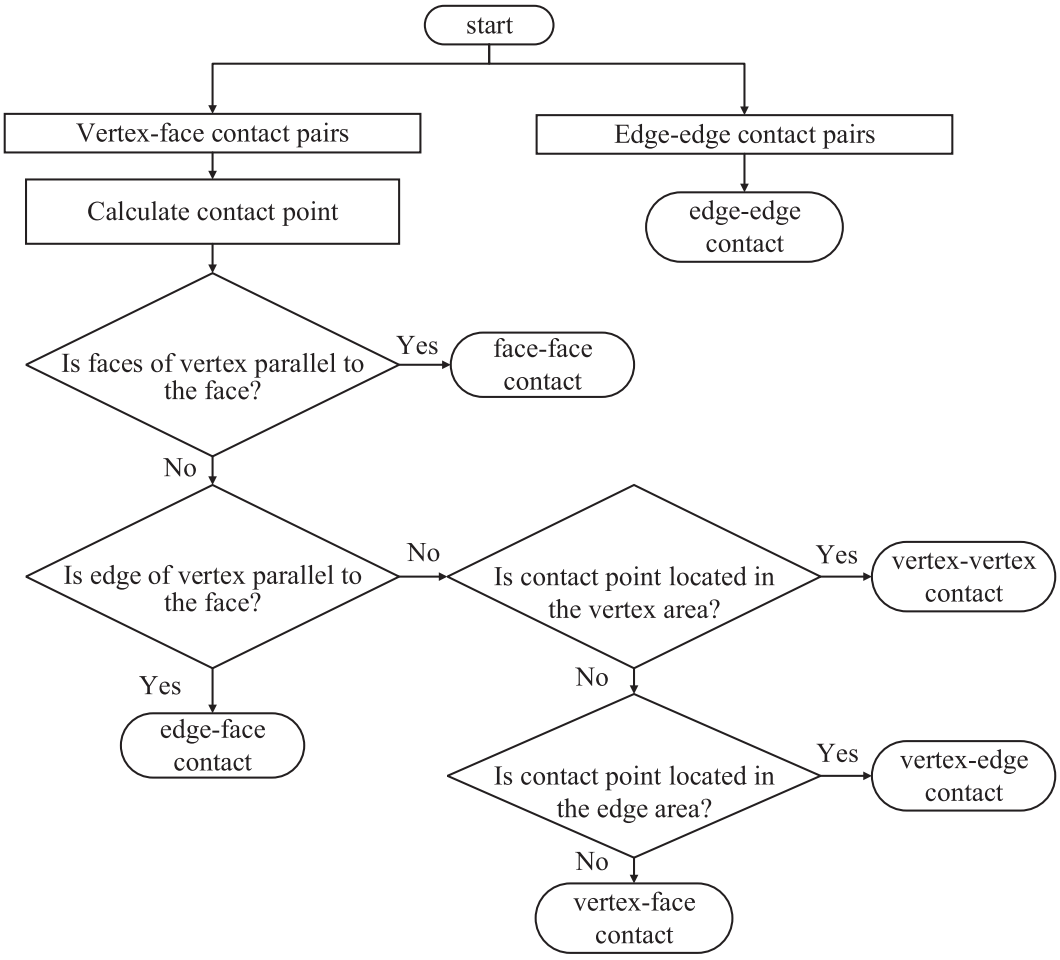

Fig. 12. Contact type recognition in 3D polyhedrons.

$$\overrightarrow{e_{vi}p_i} \cdot \overrightarrow{n_{fk}} < 0. \tag{26}$$

With the above change, adjacent blocks are not recognized as contact, thus forming initial contact pairs.

2.4.5. Half-space inclusion relation of edge and edge

For a edge-edge potential contact pair with edge $e_{vi}e_{vj}$ form polyhedron Ω_1 and edge $e_{vk}e_{vm}$ form polyhedron Ω_2, the direction vector of edge $e_{vi}e_{vj}$ is $\overrightarrow{e_{vi}e_{vj}}$, the direction vector of edge $e_{vk}e_{vm}$ is $\overrightarrow{e_{vk}e_{vm}}$. Two direction vectors normal to edge $e_{vi}e_{vj}$ in face A_{fi} and face A_{fj} are $\overrightarrow{h_{vi}}$ and $\overrightarrow{h_{vj}}$ respectively. Two direction vectors normal to edge $e_{vk}e_{vm}$ in face A_{fk} and face A_{fm} are $\overrightarrow{h_{vk}}$ and $\overrightarrow{h_{vm}}$ respectively. n_{ee} is the normal vector of the face defined by edge $e_{vi}e_{vj}$ and edge $e_{vk}e_{vm}$. If edge $e_{vi}e_{vj}$ and edge $e_{vk}e_{vm}$ satisfy

$$\overrightarrow{n_{ee}} \times \overrightarrow{h_{vi}} \leqslant 0, \overrightarrow{n_{ee}} \times \overrightarrow{h_{vj}} \leqslant 0, \overrightarrow{p_iq_i} \cdot \overrightarrow{n_{ee}} \geqslant 0, \tag{27}$$

or

$$\overrightarrow{n_{ee}} \times \overrightarrow{h_{vi}} \geqslant 0, \overrightarrow{n_{ee}} \times \overrightarrow{h_{vj}} \geqslant 0, \overrightarrow{p_iq_i} \cdot \overrightarrow{n_{ee}} \leqslant 0, \tag{28}$$

where $\overrightarrow{p_iq_i}$ is the direction vector of line form point p_i on edge $e_{vi}e_{vj}$ to point q_i on the edge $e_{vk}e_{vm}$. Then the edge $e_{vi}e_{vj}$ or the edge $e_{vk}e_{vm}$ is locate in the half-space defined by edge $e_{vi}e_{vj}$ and edge $e_{vk}e_{vm}$. The edge-edge potential contact pair satisfies the half-space inclusion relation.

For blocks that are initially stacked neatly, the tolerance to define half-space inclusion relation is altered in the first step, Eqs. (27) and (28) are changed into

$$\overrightarrow{n_{ee}} \times \overrightarrow{h_{vi}} \leqslant 0, \overrightarrow{n_{ee}} \times \overrightarrow{h_{vj}} \leqslant 0, \overrightarrow{p_iq_i} \cdot \overrightarrow{n_{ee}} > 0, \tag{29}$$

and

$$\overrightarrow{n_{ee}} \times \overrightarrow{h_{vi}} \geqslant 0, \overrightarrow{n_{ee}} \times \overrightarrow{h_{vj}} \geqslant 0, \overrightarrow{p_iq_i} \cdot \overrightarrow{n_{ee}} < 0. \tag{30}$$

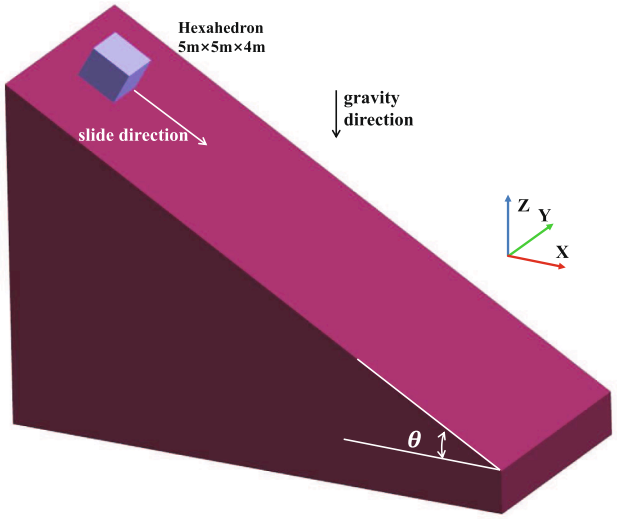

Fig. 13. Model of a slider sliding along the slope.

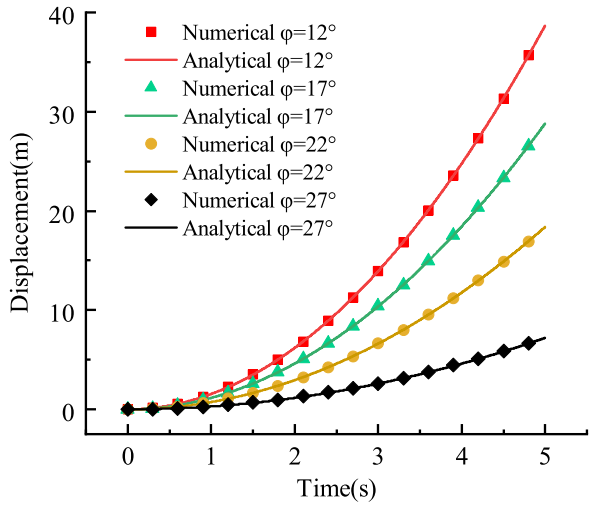

Fig. 14. The comparison between numerical results and analytical results.

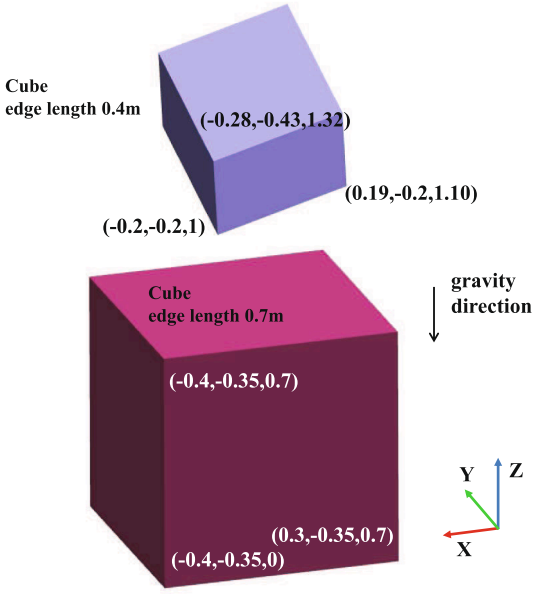

Fig. 15. Model of 3D collision blocks.

With the above changes, adjacent blocks are not recognized as contact, thus forming initial contact pairs.

2.4.6. *Contact detection*

As shown in Fig. 9 and Fig. 10, for convex polyhedrons, there is no possibility of contact between Ω_1 and Ω_2 if the vertex is located outside the half-space or the edge is located outside the edge. That is

$$\neg(\exists(\text{vertex}-\text{face}\vee\text{edge}-\text{edge satisfy half}-\text{space inclusion relation}))\Rightarrow\neg\ \text{Contact}. \tag{31}$$

Consider the relationship between original proposition and converse-negative proposition:

$$\text{Contact}\Rightarrow\forall(\text{vertex}-\text{face}\wedge\text{edge}-\text{edge satisfy half}-\text{space inclusion relation}). \tag{32}$$

Form above discussion, for polyhedrons, all the six contact type can be attributed to vertex-face contact and edge-edge contact. When two blocks do not contact, there must be vertex-face potential contact pair or edge-edge potential contact pair do not satisfy the half-space inclusion relation, that is

$$\neg\ \text{Contact}\Rightarrow\neg(\exists(\text{vertex}-\text{face}\vee\text{edge}-\text{edge satisfy half}-\text{space inclusion relation})), \tag{33}$$

therefore

$$\forall(\text{vertex}-\text{face}\wedge\text{edge}-\text{edge satisfy half}-\text{space inclusion relation})\Rightarrow\text{Contact}. \tag{34}$$

In conclusion

$$\forall\ \text{Satisfy half}-\text{space inclusion relation}\Leftrightarrow\text{Contact}. \tag{35}$$

If all potential contact pairs between two blocks satisfy the half-space inclusion relation, the two blocks are in contact. If any potential contact pair does not satisfy the half-space inclusion relation, the two blocks are in contact.

Because of the complexity of recognition and relative relation judgment of the potential contact pairs between edges, the potential contact pairs between vertices and surfaces of polyhedrons are firstly identified and judged in calculation. If all judgments between vertex and face are satisfied, then take edge-edge potential contact pairs into calculation. If any potential contact pair does not satisfy the half-space inclusion relation, it can be judged as not contact.

Specific contact type (vertex-vertex contact, vertex-edge contact, vertex -face contact, edge-edge contact, edge-face contact and face-face contact) are identified when two blocks are judged to be in contact, and the corresponding contact force is applied.

2.5. *Contact type recognition*

To simplify the contact condition detecting process, the three contact types (vertex-vertex contact, vertex-edge contact, edge-edge contact) between 2D blocks are all identified by vertex-edge potential contact pairs. The six contact types (vertex-vertex contact, vertex-edge contact, vertex -face contact, edge-edge contact, edge-face contact and face-face contact) between 3D blocks are identified by vertex-face potential contact pairs and edge-edge potential contact pairs. After the contact status is detected, it is necessary to further identify the contact types between blocks and calculate the contact position between blocks, so as to calculate the contact area and apply the corresponding contact force.

Potential contact pairs that do not satisfy the half-space inclusion relation in the previous moment of contact occurrence are initial contact

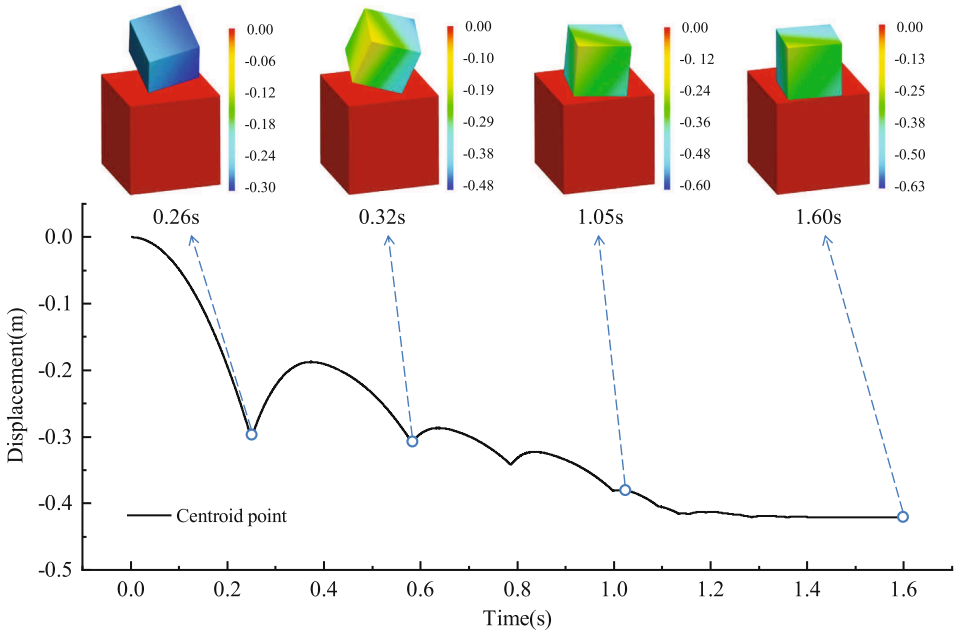

Fig. 16. Simulation results at different instants.

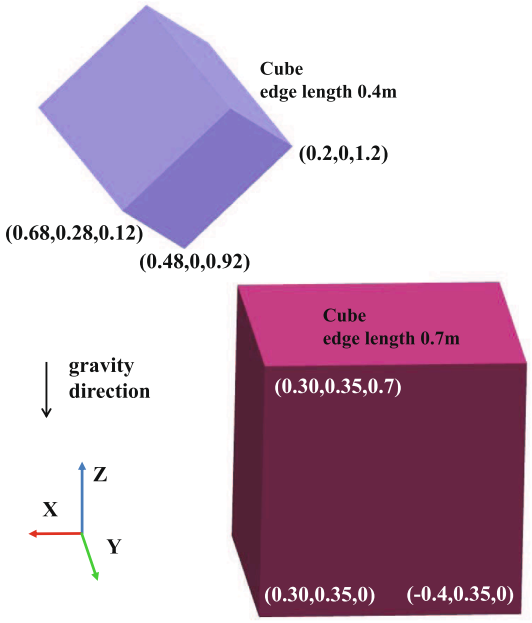

Fig. 17. Model of 3D collision blocks.

pairs. For example, if contact occurrence at time t_{n+1}, potential contact pairs that do not satisfy the half-space inclusion relation at time t_n are initial contact pairs. There may be several initial contact pairs. The specific contact type between blocks is determined by the type, number and location of initial contact pairs.

For polygons, there are only vertex-edge potential contact pairs. Fig. 11 presents the procedure of contact type recognition. The position relation between the vertex and the edge in initial contact pair is calculated to identify the specific contact type. If there is a parallel relation between vertex vector and edge vector, then edge- edge contact occurs. If there is no parallel relation, calculate the contact point between the vertex and the edge. If the contact point is located in the vertex area, the vertex-vertex contact occurs. If the contact point is located outside the vertex area, the vertex-edge contact occurs.

For polyhedrons, there are vertex-face potential contact pairs and edge-edge potential contact pairs. Fig. 12 presents the procedure of contact type recognition. If the initial contact pair is a vertex-face contact pair, calculate the specific position relation between the vertex and the face. If any face of the vertex is parallel to the corresponding face, the face-face contact occurs. If there is no face parallel, the edge of the vertex is parallel to the face, the edge-face contact occurs. If there are no parallel faces and parallel edges, then calculate the contact point between the vertex and the face. If the contact point is located in the vertex area, the vertex-vertex contact occurs. If the contact point is located on the edge areas, the vertex-edge contact occurs. If the contact point is located outside the vertex and the edge area, the vertex-face contact occurs. If the initial contact pair is edge-edge potential contact pair, the edge-edge contact occurs.

After identifying the contact type, define the contact plane for contact force calculation. For polygons, the contact plane is the edge of the half-space. For polyhedrons, the contact plane is the face of the half-space. The contact normal vector is the unit vector of the contact plane which point outside the half-space. For some special contact types, like vertex-vertex contact in polygons and vertex-edge contact in polyhedrons, the contact normal vector is the unit vector of the sum of half-spaces vector.

For hybrid continuous-discontinuous numerical methods like NMM and CDEM, blocks are initially neatly stacked. The blocks move against each other only after fracture, then the contact detection needs to be introduced. The contact area at the initial moment is the area of block boundary. When blocks fracture, the strength between blocks disappears and the contact area no longer considered.

3. Contact force

Contact force is calculate based on the penalty spring. The normal and shear contact springs are created on the contact position to calculate the contact force.

3.1. Normal contact force

Use linear penalty law to calculate normal contact force $\overrightarrow{F_n}$:

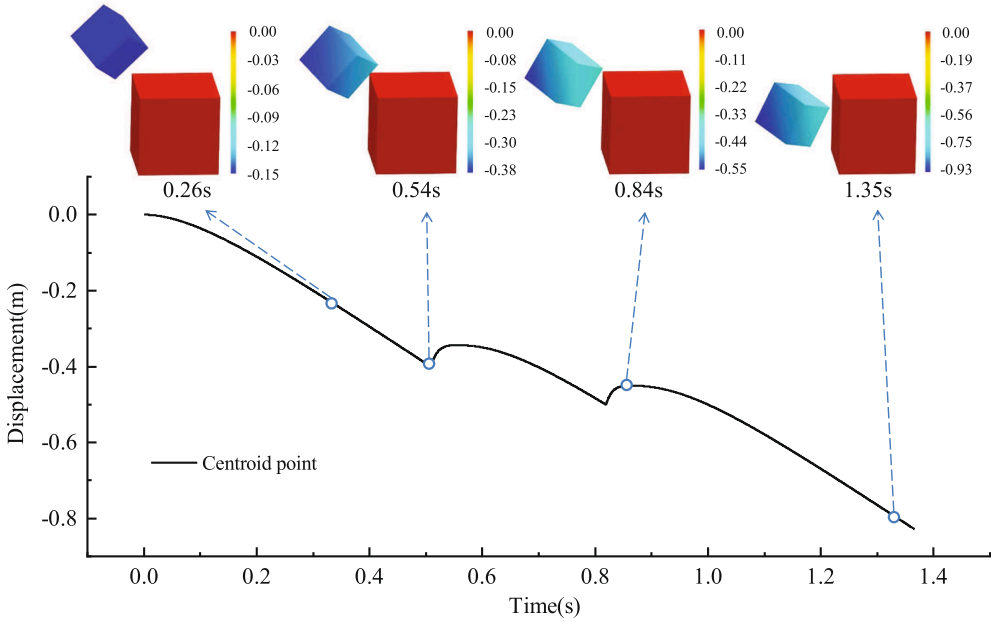

Fig. 18. Simulation results at different instants.

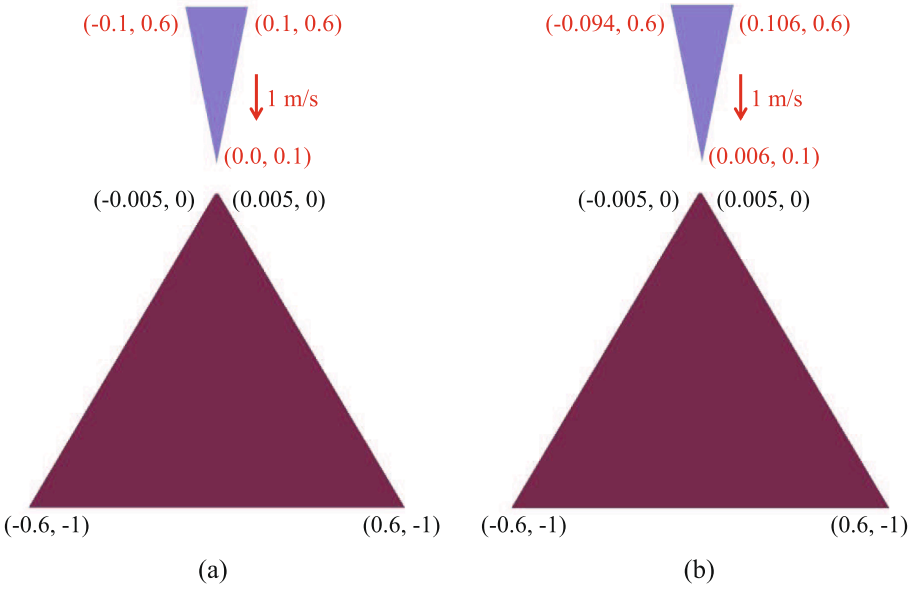

Fig. 19. Two collision cases of blocks with small edges: (a) case 1: contact of vertex and small edge; (b) case 2: contact of vertex and neighboring edge of the small edge.

$$\overrightarrow{F_n} = K_n \cdot d_n \cdot \overrightarrow{n_f}, \tag{36}$$

where K_n is the normal contact spring stiff, d_n is the normal embedded depth, $\overrightarrow{n_f}$ is the unit normal vector of the contact plane.

3.2. Shear contact force

Use incremental method is to calculate shear contact force. The shear contact force increment $\Delta\overrightarrow{F_s}$ is calculated as

$$\Delta\overrightarrow{F_s} = K_s \cdot \Delta\overrightarrow{d_s}, \tag{37}$$

where K_s is the shear contact spring stiff, $\Delta\overrightarrow{d_s}$ is the shear displacement increment.

The total shear force is the sum of current shear force increment and existing shear forces. At time $t + \Delta t$, the total shear force $\overrightarrow{F_s}(t + \Delta t)$ is calculated as

$$\overrightarrow{F_s}(t + \Delta t) = \overrightarrow{F_s}(t) + \Delta\overrightarrow{F_s} \quad \left(\overrightarrow{F_s}(t) = 0 \text{when time t do not have contact}\right). \tag{38}$$

When the shear contact force satisfies

$$|\overrightarrow{F_s}(t + \Delta t)| > |\overrightarrow{F_n}(t + \Delta t)| \cdot \tan\varphi + c \cdot A_C, \tag{39}$$

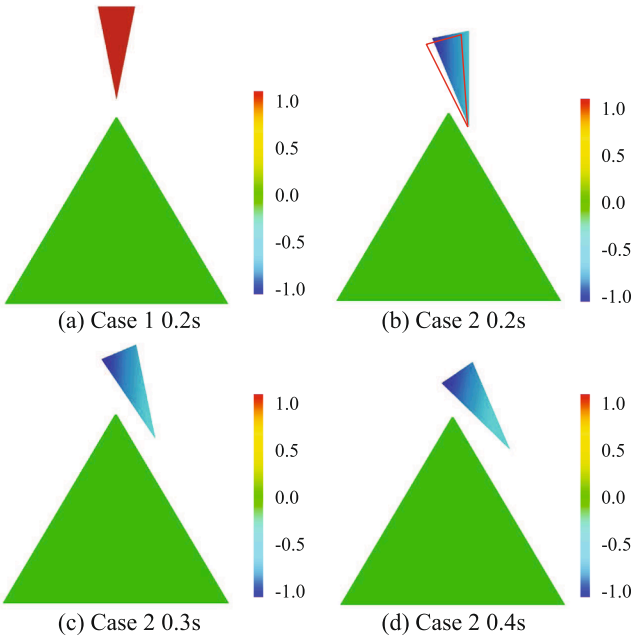

Fig. 20. Velocity at different instants: (a) result of case 1 at 0.2s; (b) result of case 2 at 0.2s (The red triangle is the result of Zheng et al. (2020b)); (c) result of case 2 at 0.3s; (d) result of. case 2 at 0.4s.

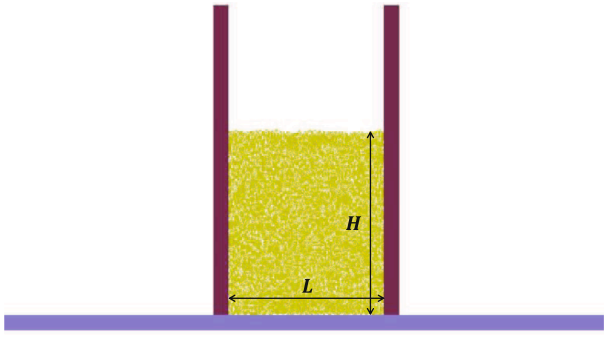

Fig. 21. Bulk material model.

where φ is the friction angle of the block, c is the cohesion of the block and A_C is the contact area, shear failure occurs, the shear contact force is updated to

$$|\overrightarrow{F_s}(t+\Delta t)| = |\overrightarrow{F_n}(t+\Delta t)|\cdot\tan\varphi. \tag{40}$$

4. Numerical cases

Spatial grid method is adopted for neighbor search. Map blocks to different cells based on their centroid. There are 8 adjacent cells in 2D space and 26 adjacent ells in 3D space, blocks in the same and adjacent cells are potential contact blocks. Detecting the contact relationship between potential contact blocks. The above-mentioned contact detection algorithm is programmed by VC++. Several examples validated the reliability and accuracy of this algorithm.

4.1. Block sliding

When a slider slides along the slope, there is friction force and supporting force between the slider and the slope. The slope angle is θ, the friction angle between the slider and the slope is φ. When the friction angle is smaller than the slope angle, the slider will move downward along the slope. According to the theoretical solution, the relationship between the displacement of the slider along the slope surface $s$and the time $t$can be expressed as:

$$s(t) = \frac{1}{2}at^2, \qquad a = g\sin\theta - g\cos\theta\cdot\tan\varphi, \tag{41}$$

where $a$is the acceleration along the slide direction, $g$is the acceleration of gravity.

The process of the slider sliding along the slope is simulated. Based on Mohr–Coulomb criterion, failure state between blocks are judged. Contact relationship and contact force are update when there is slip between blocks. The angle of slope is 30°, and the model of slider is established by a hexahedron with a length of 5m × 5m × 4m (see Fig. 13). The mechanical parameters of blocks are set as: density $\rho = 2500\text{kg/m}^3$, elastic modulus $E = 1\text{GPa}$, Poisson's ratio $\upsilon = 0.15$. The normal spring and shear spring stiffness are both $1 \times 10^{10}\text{N/m}$. The time step of numerical simulation is 10 μs, and the total calculation time is 5 s. Set the friction Angle as 15°, 20°, 25° and 30° respectively for simulated.

Compare the numerical simulation results with theoretical solutions (see Fig. 14). It can be found that the numerical calculation results are consistent with the theoretical solution. The accuracy of the algorithm for calculating 3D contact forces is verified.

4.2. Collision between two convex polyhedral blocks

The collision between 3D blocks is simulated. The model is established as shown in the Fig. 15. Block $B$is fixed, block Amoves downward under the force of gravity. The mechanical parameters of blocks are set as: density $\rho = 2500\text{kg/m}^3$, elastic modulus $E = 2\text{GPa}$, Poisson's ratio $\upsilon = 0.2$, friction angle $\varphi = 30°$. The normal spring and shear spring stiffness are both $2 \times 10^{10}\text{N/m}$. The time step of numerical simulation is 10μs.

Block $A$is in free fall and then bounced off after contact with block B, and finally falls steadily on block B. The vertical displacement during the movement of the block are shown in the Fig. 16. The accuracy of vertex-face contact, edge-face contact and face-face contact occur during the falling process is verified.

The model as shown in the Fig. 17 is established. The block D is fixed, while block C moves downward under the force of gravity. The mechanical parameters of blocks are set as: density $\rho = 2500\text{kg/m}^3$, elastic modulus $E = 20\text{GPa}$, Poisson's ratio $\upsilon = 0.2$, friction angle $\varphi = 30°$. The normal spring and shear spring stiffness are both $2 \times 10^{11}\text{N/m}$. The time step of numerical simulation is 10μs. The vertical displacement during the movement of the block are shown in the Fig. 18. Block A bounced off after the edge of block A contacts with the edge of block B, and then continues to move downward. The accuracy of edge-edge contact is verified.

4.3. Block with small edges

Two collision cases for blocks with small edges are simulated. This validation case is the same as one of the cases in Zheng's article (Zheng et al., 2020b). Two models are established as shown in the Fig. 19. For case 1, the vertex of the upper block will contact with the small edge. For case 2, the vertex of the upper block will contact the edge to the right of the small edge. The mechanical parameters of blocks are set as: density $\rho = 2000\text{kg/m}^3$, elastic modulus $E = 1\text{GPa}$, Poisson's ratio $\upsilon = 0.25$. The normal spring stiffness is $5 \times 10^6\text{N/m}$ and shear spring stiffness is $1 \times 10^6\text{N/m}$. The time step of numerical simulation is 20 μs.

The vertical velocity during the movement of the block are shown in the Fig. 20. For case 1, the upper block collides with the small edge and then moves upward vertically. For case 2, the upper block collides with the edge right to the small edge and then moves to the right side. The

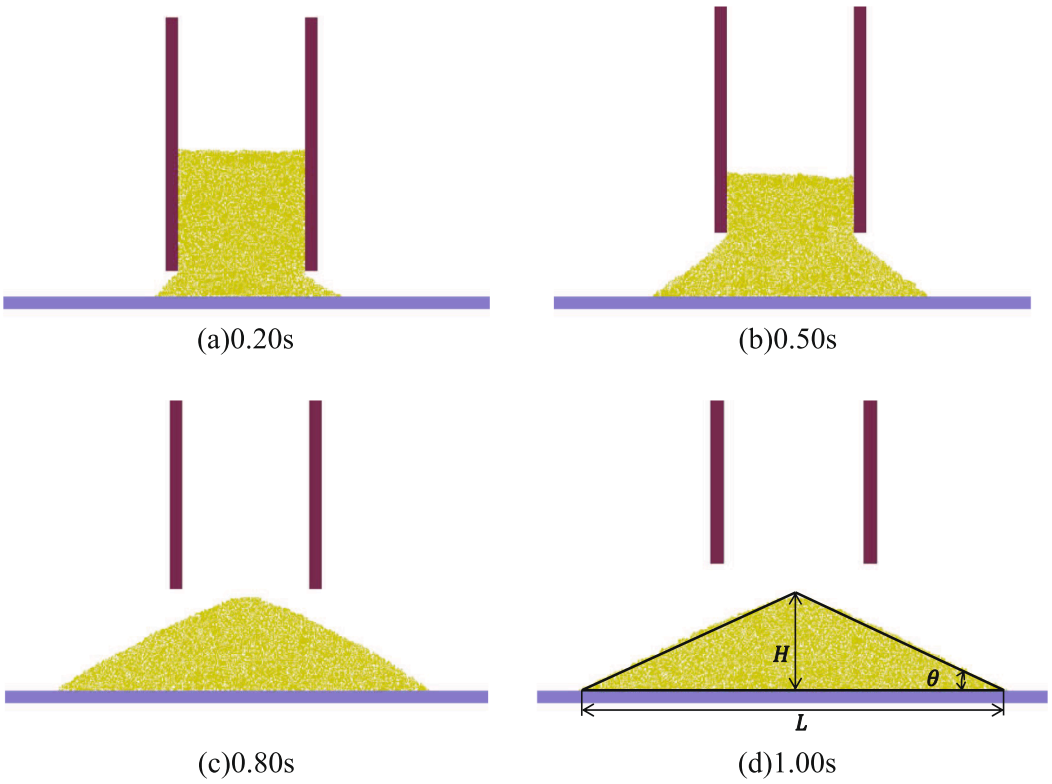

Fig. 22. Simulation of the angle of repose.

simulation result of case 2 at 0.2s is compared with Zheng's result. The movement of the vertex is identical. Robustness of this algorithm for blocks with small edges is verified.

4.4. Measurement of the angle of repose

The measurement process of the angle of repose of bulk material is simulated. The bulk material model is established as shown in the Fig. 21. The width *L*of bulk material is 1m and the height *H*is 1.2m. A bottom plate is set at the bottom of the bulk material, and baffles are set on both sides of the bulk material, the thickness of the bottom plate and the baffles is 0.1m. The material is meshed by 5788 triangular elements with an average size of 0.02m. The bottom plate and baffles is meshed by 440 quadrilateral elements with a size of 0.05m to divide this area.

The mechanical parameters of material are set as: density $\rho = 2500\text{kg/m}^3$, elastic modulus $E = 10\text{MPa}$, Poisson's ratio $\upsilon = 0.3$, friction angle $\varphi = 25^{\circ}$, cohesion $C = 0\text{MPa}$. The time step of numerical simulation is 10 μs. The mechanical parameters between the material and the baffles are set as: friction angle $\varphi_b = 0^{\circ}$, cohesion $C = 0\text{MPa}$. The mechanical parameters between the material and the bottom plate are set as: friction angle $\varphi_c = 25^{\circ}$, cohesion $C = 0\text{MPa}$. The normal spring and shear spring stiffness are both $1 \times 10^8\text{N/m}$. The time step of numerical simulation is 20 μs.

Taking the measurement procedure of the angle of repose for reference (Chen et al., 2015), the baffles on both sides move upward at a speed of 0.1m/s. As the baffles rise, the material flows out from both sides. When calculated to 1.0s, the material reaches a stable state, forming a certain accumulation angle, as shown in the Fig. 22 The repose angle θ of the accumulation body is 25°, same as the set friction angle between the material. The accuracy of this algorithm in calculating the 2D problem is verified.

5. Conclusion

This paper presented a new contact detection algorithm to detect the contact status between convex polygons and convex polyhedrons. Two conceptions are proposed for the contact detection: potential contact pairs and half-space inclusion relation. This contact detection algorithm determines contact status between two blocks by judging half-space inclusion relation. Potential contact pairs are identified by the relation between face normal vector and vertex vectors. Vertex-edge potential contact pairs are defined for polygons, vertex-face potential contact pairs and edge-edge potential contact pairs are defined for polyhedrons. Half-space inclusion relation is the relative positional relation between the two geometry elements in potential contact pair. The three contact types between polygon are all detected through vertex-edge potential contact pairs, and the six contact types between polyhedrons are all detected through vertex -face potential contact pairs and edge-edge potential contact pairs, thus simplifying the progress of contact detection. Potential contact pairs and half-space inclusion relation are both identified by the calculate of vectors, distance calculation between blocks are not involved in the progress of contact status detection.

Simulation results validate the accuracy and robustness of this algorithm. Several cases are given to verify that all contact types between two convex polygons or two convex polyhedrons can be recognized through the basic potential contact pairs, and collision of polygons with small edges can be detected. The accuracy of this algorithm is verified by the simulation results.

This contact detection algorithm can also be used to detect the contact between concave blocks which is still in development.

Declaration of Competing Interest

The authors declare that they have no known competing financial interests or personal relationships that could have appeared to influence

the work reported in this paper.

Acknowledgment

The authors would like to acknowledge the financial support of the National Key Research and Development Project of China, the Ministry of Science and Technology of China (Project No. 2018YFC1505504).

References

Aceituno, B., Mastalli, C., Dai, H., Focchi, M., Radulescu, A., Caldwell, D., Cappelletto, J., Grieco, J., Fernandez, G., Semini, C., 2018. Simultaneous contact, gait and motion planning for robust multi-legged locomotion via mixed-integer convex optimization. IEEE Robot. Autom. Lett. 25, 1–8. https://doi.org/10.1109/LRA.2017.2779821.

Barki, H., Denis, F., Dupont, F., 2009. Contributing vertices-based minkowski sum computation of convex polyhedra. Comput. Aided Des. 41, 525–538. https://doi.org/10.1016/j.cad.2009.03.008.

Barraquand, J., Latombe, J.C., 1991. Robot motion planning: A distributed representation approach. Int. J. Rob. Res. 10, 628–649. https://doi.org/10.1177/027836499101000604.

Bekker, H., Roerdink, J.B.T.M., 2001. An efficient algorithm to calculate the minkowski sum of convex 3d polyhedra. In: Proceedings of the International Conference on Computational Sciences-Part I. Springer-Verlag, Berlin, Heidelberg, pp. 619–628. https://doi.org/10.1007/3-540-45545-0_71.

Boon, C.W., Houlsby, G.T., Utili, S., 2012. A new algorithm for contact detection between convex polygonal and polyhedral particles in the discrete element method. Comput. Geotech. 44, 73–82. https://doi.org/10.1016/j.compgeo.2012.03.012.

Boon, C.W., Houlsby, G.T., Utili, S., 2013. A new contact detection algorithm for three-dimensional non-spherical particles. Powder Technol. 248, 94–102. https://doi.org/10.1016/j.powtec.2012.12.040.

Bovet, S., Debarba, H.G., Herbelin, B., Molla, E., Boulic, R., 2018. The critical role of self-contact for embodiment in virtual reality. IEEE Trans. Vis. Comput. Graph. 24, 1428–1436. https://doi.org/10.1109/TVCG.2018.2794658.

Chen, H., Liu, Y.L., Zhao, X.Q., Xiao, Y.G., Liu, Y., 2015. Numerical investigation on angle of repose and force network from granular pile in variable gravitational environments. Powder Technol. 283, 607–617. https://doi.org/10.1016/j.powtec.2015.05.017.

Coussot, P., Meunier, M., 1996. Recognition, classification and mechanical description of debris flows. Earth Sci. Rev. 40, 209–227. https://doi.org/10.1016/0012-8252(95)00065-8.

Cundall, P.A., 1971. A computer model for simulating progressive, large-scale movements in block rock systems. Proc. Int. Symp. Rock Frac. 1 (II-B), 11–18.

Cundall, P.A., 1988. Formulation of a three-dimensional distinct element model–part i. a scheme to detect and represent contacts in a system composed of many polyhedral blocks. Int. J. Rock Mech. Min. Sci. 25, 289. https://doi.org/10.1016/0148-9062(88)91214-4.

Cundall, P.A., Strack, O.D.L., 1979. A discrete numerical model for granular assemblies. Géotechnique 29, 47–65. https://doi.org/10.1680/geot.1979.29.1.47.

Davies, T., McSaveney, M., 2009. The role of rock fragmentation in the motion of large landslides. Eng. Geol. 109, 67–79. https://doi.org/10.1016/j.enggeo.2008.11.004.

Fan, H., Zheng, H., Wang, J., 2018. A generalized contact potential and its application in discontinuous deformation analysis. Comput. Geotech. 99, 104–114. https://doi.org/10.1016/j.compgeo.2018.02.023.

Feng, C., Li, S., Liu, X., Zhang, Y., 2014. A semi-spring and semi-edge combined contact model in cdem and its application to analysis of jiweishan landslide. J. Rock Mech. Geotech. Eng. 6, 26–35. https://doi.org/10.1016/j.jrmge.2013.12.001.

Garbaya, S., Zaldivar-Colado, U., 2007. The affect of contact force sensations on user performance in virtual assembly tasks. Virtual Real. 11, 287–299. https://doi.org/10.1007/s10055-007-0075-5.

Gilbert, E., Johnson, D., Keerthi, S., 1987. A fast procedure for computing the distance between complex objects in three space, in. In: Proceedings. 1987 IEEE International Conference on Robotics and Automation, pp. 1883–1889. https://doi.org/10.1109/ROBOT.1987.1087825.

Hatzor, Y.H., Ma, G., Shi, G.H., 2017. Discontinuous Deformation Analysis in Rock Mechanics Practice. CRC Press. https://doi.org/10.4324/9781315687032.

Jafari, A., Keneti, A.R., 2013. Improvement of contact detection in 'approaching faces' method for use in three-dimensional discontinuous deformation analysis. Min. Technol. 116, 79–87. https://doi.org/10.1179/174328607x198923.

Khishvand, M., Nazem, M., Sloan, S.W., Carter, J.P., 2017. Application of the third medium method for frictionless contact problems in geomechanics. Comput. Geotech. 85, 117–125. https://doi.org/10.1016/j.compgeo.2016.12.020.

Li, S., Tang, D., Wang, J., 2015. A two-scale contact model for collisions between blocks in cdem. Sci. China Technol. Sci. 58, 1596–1603. https://doi.org/10.1007/s11431-015-5902-4.

Lin, Q., Li, S., Feng, C., Wang, X., 2021. Cohesive fracture model of rocks based on multi-scale model and lennard-jones potential. Eng. Fract. Mech. 246, 107627. https://doi.org/10.1016/j.engfracmech.2021.107627.

Liu, X., Lemos, J., 2001. Procedure for contact detection in discrete element analysis. Adv. Eng. Softw.e 32, 409–415. https://doi.org/10.1016/S0965-9978(00)00101-0.

Lubbe, R., Xu, W.J., Wilke, D.N., Pizette, P., Govender, N., 2020. Analysis of parallel spatial partitioning algorithms for gpu based dem. Comput. Geotech. 125, 103708. https://doi.org/10.1016/j.compgeo.2020.103708.

Mai, S., Gravouil, A., Nguyen-Tajan, M., Trollé, B., 2017. Numerical simulation of rolling contact fatigue crack growth in rails with the rail bending and the frictional contact. Eng. Fract. Mech. 174, 19–206. https://doi.org/10.1016/j.engfracmech.2016.12.019.

Marques, F., Magalhães, H., Pombo, J., Ambrósio, J., Flores, P., 2020. A three-dimensional approach for contact detection between realistic wheel and rail surfaces for improved railway dynamic analysis. Mech. Mach. Theory 149, 1–28. https://doi.org/10.1016/j.mechmachtheory.2020.103825.

Mu, L., Zhang, Y., 2020. Cracking elements method with 6-node triangular element. Finite Elem. Anal. Des. 177, 103421. https://doi.org/10.1016/j.finel.2020.103421.

Nezami, E.G., Hashash, Y.M.A., Zhao, D., Ghaboussi, J., 2004. A fast contact detection algorithm for 3-d discrete element method. Comput. Geotech. 31, 575–587. https://doi.org/10.1016/j.compgeo.2004.08.002.

Nezami, E.G., Hashash, Y.M.A., Zhao, D., Ghaboussi, J., 2006. Shortest link method for contact detection in discrete element method. Int. J. Numer. Anal. Methods Geomech. 30, 783–801. https://doi.org/10.1002/nag.500.

Park, J.W., Song, J.J., 2009. Numerical simulation of a direct shear test on a rock joint using a bonded-particle model. Int. J. Rock Mech. Min. Sci. 46, 1315–1328. https://doi.org/10.1016/j.ijrmms.2009.03.007.

Peng, D., Hanley, K.J., 2019. Contact detection between convex polyhedra and superquadrics in discrete element codes. Powder Technol. 356, 11–20. https://doi.org/10.1016/j.powtec.2019.07.082.

Redon, S., Kheddar, A., Coquillart, S., 2010. Fast continuous collision detection between rigid bodies. Comput. Graph. Forum. 21, 279–287. https://doi.org/10.1111/1467-8659.t01-1-00587.

Römer, U.J., Fidlin, A., Seemann, W., 2018. Explicit analytical solutions for two-dimensional contact detection problems between almost arbitrary geometries and straight or circular counterparts. Mech. Mach. Theory 128, 205–224. https://doi.org/10.1016/j.mechmachtheory.2018.05.018.

Shi, G., 1992. Discontinuous deformation analysis: A new numerical model for the statics and dynamics of deformable block structures. Eng. Comput. 9, 157–168. https://doi.org/10.1108/eb023855.

Shi, G., 2015. Contact theory. Sci. China Technol. Sci. 58, 1450–1496. https://doi.org/10.1007/s11431-015-5814-3.

Shire, T., Hanley, K.J., Stratford, K., 2020. Dem simulations of polydisperse media: efficient contact detection applied to investigate the quasi-static limit. Comput. Part. Mech. 1–11. https://doi.org/10.1007/s40571-020-00361-2.

Stühler, S., Fleissner, F., Eberhard, P., 2016. A contact detection algorithm for deformable tetrahedral geometries based on a novel approach for general simplices used in the discrete element method. Comput. Part. Mech. 5, 35–47. https://doi.org/10.1007/s40571-016-0147-y.

Tan, X., Konietzky, H., Chen, W., 2016. Numerical simulation of heterogeneous rock using discrete element model based on digital image processing. Rock Mech. Rock Eng. 49, 4957–4964. https://doi.org/10.1007/s00603-016-1030-0.

Varadhan, G., Manocha, D., 2006. Accurate minkowski sum approximation of polyhedral models. Graph. Models 68, 343–355. https://doi.org/10.1016/j.gmod.2005.11.003.

Wang, J., Li, S., Feng, C., 2015. A shrunken edge algorithm for contact detection between convex polyhedral blocks. Comput. Geotech. 63, 315–330. https://doi.org/10.1016/j.compgeo.2014.10.009.

Wang, X., Wu, W., Zhu, H., Lin, J.S., Zhang, H., 2019. Contact detection between polygonal blocks based on a novel multi-cover system for discontinuous deformation analysis. Comput. Geotech. 111, 56–65. https://doi.org/10.1016/j.compgeo.2019.03.004.

Wang, X., Wu, W., Zhu, H., Lin, J.S., Zhang, H., 2020. Acceleration of contact detection between arbitrarily shaped polyhedra based on multi-cover methods in three dimensional discontinuous deformation analysis. Int. J. Rock Mech. Min. Sci. 132, 104387. https://doi.org/10.1016/j.ijrmms.2020.104387.

Wang, X., Wu, W., Zhu, H., Zhang, H., Lin, J.S., 2020. The last entrance plane method for contact indeterminacy between convex polyhedral blocks. Comput. Geotech. 117, 103238. https://doi.org/10.1016/j.compgeo.2019.103283.

Wu, J.H., 2008. New edge-to-edge contact calculating algorithm in three-dimensional discrete numerical analysis. Adv. Eng. Softw.e 39, 15–24. https://doi.org/10.1016/j.advengsoft.2006.11.007.

Yang, P., Zang, M., Zeng, H., 2020. An efficient 3d dem-fem contact detection algorithm for tire-sand interaction. Powder Technol. 360, 1102–1116. https://doi.org/10.1016/j.powtec.2019.10.069.

Zhang, H., Liu, S.G., Han, Z., Zheng, L., Zhang, Y.B., Wu, Y.Q., Li, Y.G., Wang, W., 2016. A new algorithm to identify contact types between arbitrarily shaped polyhedral blocks for three-dimensional discontinuous deformation analysis. Comput. Geotech. 80, 1–15. https://doi.org/10.1016/j.compgeo.2016.06.007.

Zhang, Q., Zhi, Z., Feng, C., Cai, Y., Pang, G., Yue, J., 2020. Investigation of concrete pavement cracking under multi-head impact loading via the continuum-discontinuum element method. Int. J. Impact Eng. 135, 103410. https://doi.org/10.1016/j.ijimpeng.2019.103410.

Zhang, X., Redon, S., Lee, M., Kim, Y.J., 2007. Continuous collision detection for articulated models using taylor models and temporal culling. ACM Trans. Graph. 26, 1–10. https://doi.org/10.1145/1276377.1276396.

Zhang, Y., Gao, Z., Li, Y., Zhuang, X., 2020. On the crack opening and energy dissipation in a continuum based disconnected crack model. Finite Elem. Anal. Des. 170, 103333. https://doi.org/10.1016/j.finel.2019.103333.

Zhang, Y., Mang, H.A., 2020. Global cracking elements: A novel tool for galerkin-based approaches simulating quasi-brittle fracture. Int. J. Numer. Methods Eng. 121, 2462–2480. https://doi.org/10.1002/nme.6315.

Zhang, Y., Zhuang, X., 2018. Cracking elements: A self-propagating strong discontinuity embedded approach for quasi-brittle fracture. Finite Elem. Anal. Des. 144, 84–100. https://doi.org/10.1016/j.finel.2017.10.007.

Zhang, Y., Zhuang, X., 2019. Cracking elements method for dynamic brittle fracture. Theor. Appl. Fract. Mech. 102, 1–9. https://doi.org/10.1016/j.tafmec.2018.09.015.
Zheng, F., Jiao, Y.Y., Gardner, M., Sitar, N., 2017a. A fast direct search algorithm for contact detection of convex polygonal or polyhedral particles. Comput. Geotech. 87, 76–85. https://doi.org/10.1016/j.compgeo.2017.02.001.
Zheng, F., Jiao, Y.Y., Leung, Y.F., Zhu, J., 2018a. Algorithmic robustness for contact analysis of polyhedral blocks in discontinuous deformation analysis framework. Comput. Geotech. 104, 288–301. https://doi.org/10.1016/j.compgeo.2018.07.019.
Zheng, F., Jiao, Y.Y., Sitar, N., 2018b. Generalized contact model for polyhedra in three-dimensional discontinuous deformation analysis. Int. J. Numer. Anal. Methods Geomech. 42, 1471–1492. https://doi.org/10.1002/nag.2798.
Zheng, F., Jiao, Y.Y., Zhang, X.L., Tan, F., Wang, L., Zhao, Q., 2017b. Object-oriented contact detection approach for three-dimensional discontinuous deformation analysis based on entrance block theory. Int. J. Geomech. 17, E4016009. https://doi.org/10.1061/(asce)gm.1943-5622.0000718.
Zheng, F., Leung, Y.F., Zhu, J.B., Jiao, Y.Y., 2019. Modified predictor-corrector solution approach for efficient discontinuous deformation analysis of jointed rock masses. Int. J. Numer. Anal. Methods Geomech. 43, 599–624. https://doi.org/10.1002/nag.2881.
Zheng, F., Zhuang, X., Zheng, H., Jiao, Y.Y., Rabczuk, T., 2020a. Kinetic analysis of polyhedral block system using an improved potential-based penalty function approach for explicit discontinuous deformation analysis. Appl. Math. Model. 82, 314–335. https://doi.org/10.1016/j.apm.2020.01.026.
Zheng, F., Zhuang, X., Zheng, H., Jiao, Y.Y., Rabczuk, T., 2020b. A robust potential-based contact force solution approach for discontinuous deformation analysis of irregular convex polygonal block/particle systems. Acta Geotech. 16, 679–697. https://doi.org/10.1007/s11440-020-00997-7.
Zhong, Z.H., Nilsson, L., 1989. A contact searching algorithm for general contact problems. Comput. Struct. 33, 197–209. https://doi.org/10.1016/0045-7949(89)90141-7.
Zhou, W., Huang, Y., Ng, T.T., Ma, G., 2018. A geometric potential-based contact detection algorithm for egg-shaped particles in discrete element modeling. Powder Technol. 327, 152–162. https://doi.org/10.1016/j.powtec.2017.12.053.
Zhuang, X., Zheng, F., Zheng, H., Jiao, Y., Rabczuk, T., Wriggers, P., 2020. A cover-based contact detection approach for irregular convex polygons in discontinuous deformation analysis. Int. J. Numer. Anal. Methods Geomech. 45, 208–233. https://doi.org/10.1002/nag.3157.